than in the rest of the disk. The correlation remains notable even if we do not apply a thickness filter to the data or if we use another definition of the thickness (3, 11). The two maps are not independent, however; changing the density distribution in the arms will necessarily produce changes in the measured thickness unless the perturbations are distributed in the same way as the initial distribution. The alignment of overdensities with regions of reduced thickness was suggested previously (3). This alignment has not been observed in other galaxies because surface density maps are most easily made for face-on galaxies where there is no information about the thickness of the gas layer.

The radial profile of the HI disk has been a matter of controversy for many years. A sharp falloff in HI emission as a function of velocity has long been known (*18*), but this need not correspond to an abrupt radial cutoff in the disk density (*19*). Velocity dispersion will cause features to be smeared along the line of sight by confusing the velocity-distance transformation, resulting in the radially elongated features near the edges of maps (Fig. 3). The radial extent of the spiral arms provides a minimum cutoff radius for the Galactic gas disk; in other words, it is not possible for the gas to have spiral structure beyond where the HI disk ends. This radius is only a lower limit, because it is possible that there is gas beyond where the spiral structure ends that does not participate in the spiral structure or that past some radius the arms are too weak to be detected by the unsharp masking. Near 25-kpc Galactocentric radius, both the surface density and the thickness perturbation maps (Fig. 3) change from spiral patterns to features elongated along the line of sight. This is most clearly seen in the south; the transition radius is not immediately obvious in the north. Thus, the HI gas disk must extend to at least 25 kpc from the Galactic center in the south, about three times the Sun-Galactic center distance. A related conclusion is that gas within the cutoff radius is kinematically settled into a disk; otherwise it would be unlikely to respond to the spiral density waves.

It is useful to fit four-armed models to our density perturbation map. We used logarithmic spiral arms that start at the Solar circle:

$$\log(R/R_0) = [\phi(R) - \phi_0]\tan\psi \qquad (2)$$

where ψ is the pitch angle and ϕ_0 is the Galactocentric azimuth at the Solar circle. Our fitting method was designed to trace the regions of gas overdensity. For each of the four arms apparent in Fig. 1, we investigated an evenly spaced grid of these two free parameters for ranges of values that connect the overdense contours. For each combination of ψ and ϕ_0, we linearly interpolated the value of Π for the locus of points along each arm. Any points that fall in the excluded regions were ignored. We used the median of the list of interpolated values as a measure of the goodness of fit for each curve. In this scheme, arms with values of ψ and ϕ_0 that trace overdense regions will naturally have a large median and thus a large goodness of fit. The best fit values of ψ and ϕ_0 for each of the four arms are given (Table 1). Other fits that connect a different set of features in the map could be drawn, because assigning a unique arm pattern to a map is not possible. We find pitch angles for the outer arms in the range from 20° to 25°; this is larger than the value of $\psi \approx 13°$ averaged over a variety of tracers (*20*). This does not necessarily imply a disagreement, however, because the arms could be unwinding in their outer regions.

Various models of the locations of the arms have been proposed. We compared our map to a model derived from regions of ionized hydrogen (*21–23*); the model consists of two pairs of mirror symmetric arms following logarithmic spirals. We denoted this as the symmetric model (Fig. 4). The symmetric model fits Π reasonably well over much of the southern sky; the agreement is poor in the north where the spiral structure is less prominent, possibly because of the larger thickness of the northern gas (*11*). Gas that is dynamically warmer is less likely to respond to spiral density waves, and the azimuthally averaged thickness of the northern gas is nearly twice that of the southern gas at $R = 20$ kpc.

There are several places where the symmetric model deviates from the data. For example, the arm in the north ($R \approx 13$ kpc) falls in between two of the model's arms; forcing the arms to be mirror-imaged pairs is too strong a restriction. Features near the excluded regions could result from a large-scale ordered velocity structure that has not been included in our rotation model. Elliptical streamlines with $m = 2$ could cause such an effect (*11*). Images of other galaxies suggest that the spiral arms may bifurcate into spurs in the outer disk. The structure of the Perseus and Carina arms past $R \approx 20$ kpc is suggestive of this behavior.

References and Notes

1. H. C. van de Hulst, C. A. Muller, J. H. Oort, *Bull. Astron. Inst. Neth.* **12**, 117 (1954).
2. F. Kerr, G. Westerhout, in *Galactic Structure*, vol. 5 of *Stars and Stellar Systems*, A. Blaauw, M. Schmidt, Eds. (Univ. Chicago Press, Chicago, IL, 1965), pp. 167–202.
3. A. P. Henderson, P. D. Jackson, F. J. Kerr, *Astrophys. J.* **263**, 116 (1982).
4. D. Malin, *Am. Astron. Soc. Photo Bull.* **16**, 10 (1977).
5. P. M. W. Kalberla *et al.*, *Astron. Astrophys.* **440**, 775 (2005).
6. D. Hartmann, W. B. Burton, *Atlas of Galactic Neutral Hydrogen* (Cambridge Univ. Press, Cambridge, 1997).
7. E. Bajaja *et al.*, *Astron. Astrophys.* **440**, 767 (2005).
8. E. M. Arnal, E. Bajaja, J. J. Larrarte, R. Morras, W. G. L. Pöppel, *Astron. Astrophys. Suppl. Ser.* **142**, 35 (2000).
9. M. J. Reid, *Annu. Rev. Astron. Astrophys.* **31**, 345 (1993).
10. R. P. Olling, M. R. Merrifield, *Mon. Not. R. Astron. Soc.* **297**, 943 (1998).
11. E. S. Levine, L. Blitz, C. Heiles, *Astrophys. J.* **643**, 881 (2006).
12. N. M. McClure-Griffiths, J. M. Dickey, B. M. Gaensler, A. J. Green, *Astrophys. J.* **607**, L127 (2004).
13. J. S. Miller, *Astrophys. J.* **151**, 473 (1968).
14. Y. Xu, M. J. Reid, X. W. Zheng, K. M. Menten, *Science* **311**, 54 (2006); published online 7 December 2005 (10.1126/science.1120914).
15. W. B. Burton, *Astron. Astrophys.* **10**, 76 (1971).
16. M. A. Tuve, S. Lundsager, *Astron. J.* **77**, 652 (1972).
17. C. Yuan, *Astrophys. J.* **158**, 871 (1969).
18. N. H. Dieter, *Astron. Astrophys.* **12**, 59 (1971).
19. G. R. Knapp, S. D. Tremaine, J. E. Gunn, *Astron. J.* **83**, 1585 (1978).
20. J. P. Vallée, *Astron. J.* **130**, 569 (2005).
21. W. W. Morgan, A. E. Whitford, A. D. Code, *Astrophys. J.* **118**, 318 (1953).
22. Y. M. Georgelin, Y. P. Georgelin, *Astron. Astrophys.* **49**, 57 (1976).
23. R. J. Wainscoat, M. Cohen, K. Volk, H. J. Walker, D. E. Schwartz, *Astrophys. J. Suppl. Ser.* **83**, 111 (1992).

24. We thank P. Kalberla for providing a copy of the LAB HI survey and J. Peek, C. Laver, and T. Robishaw for helpful advice regarding plots. E.S.L. and L.B. were supported by NSF grant AST 02-28963. C.H. was supported by NSF grant AST 04-06987.

7 April 2006; accepted 22 May 2006
Published online 1 June 2006;
10.1126/science.1128455
Include this information when citing this paper.

Optical Conformal Mapping

Ulf Leonhardt

An invisibility device should guide light around an object as if nothing were there, regardless of where the light comes from. Ideal invisibility devices are impossible, owing to the wave nature of light. This study develops a general recipe for the design of media that create perfect invisibility within the accuracy of geometrical optics. The imperfections of invisibility can be made arbitrarily small to hide objects that are much larger than the wavelength. With the use of modern metamaterials, practical demonstrations of such devices may be possible. The method developed here can also be applied to escape detection by other electromagnetic waves or sound.

According to Fermat's principle (*1*), light rays take the shortest optical paths in dielectric media, where the refractive index n integrated along the ray trajectory defines the path length. When n is spatially varying, the shortest optical paths are not straight lines, but are curved. This light bending is the cause of many optical illusions. Imagine a situation where a medium guides light around a hole in it. Suppose that all parallel bundles of incident rays are bent around the hole and recombined in precisely the same direction as they entered the medium. An

observer would not see the difference between light passing through the medium or propagating across empty space (or, equivalently, in a uniform medium). Any object placed in the hole would be hidden from sight. The medium would create the ultimate optical illusion: invisibility (*2*).

However, it has been proved (*3*, *4*) that perfect invisibility is unachievable, except in a finite set of discrete directions where the object appears to be squashed to infinite thinness and for certain objects that are small as compared with the wavelength (*5*, *6*). In order to carry images, though, light should propagate with a continuous range of spatial Fourier components, i.e., in a range of directions. The mathematical reason for the impossibility of perfect invisibility is the uniqueness of the inverse-scattering problem for waves (*3*): the scattering data, i.e., the directions and amplitudes of the transmitted plane-wave components determine the spatial profile of the refractive index (*3*). Therefore, the scattering data of light in empty space are only consistent with the propagation through empty space. Perfect illusions are thus thought to be impossible due to the wave nature of light.

On the other hand, the theorem (*3*) does not limit the imperfections of invisibility—they may be very small—nor does it apply to light rays, i.e., to light propagation within the regime of geometrical optics (*1*). This study develops a general recipe for the design of media that create perfect invisibility for light rays over a continuous range of directions. Because this method is based on geometrical optics (*1*), the inevitable imperfections of invisibility can be made exponentially small for objects that are much larger than the wavelength of light.

To manufacture a dielectric invisibility device, media are needed that possess a wide range of the refractive index in the spectral domain where the device should operate. In particular, Fermat's Principle (*1*) seems to imply that $n < 1$ in some spatial regions, because only in this case the shortest optical paths may go around the object without causing phase distortions. In our example, n varies from 0 to about 36. In practice, one could probably accept a certain degree of visibility that substantially reduces the demands on the range of the refractive index.

Extreme values of n occur when the material is close to resonance with the electromagnetic field. Metamaterials (*7*) with man-made resonances can be manufactured with appropriately designed circuit boards, similar to the ones used for demonstrating negative refraction (*8*). The quest for the perfect lens (*9*) has led to recent improvements (*7*, *10*–*13*) mainly focused on tuning the magnetic susceptibilities. In such metamaterials, each individual circuit plays the role of an artificial atom with tunable resonances. With these artificial dielectrics, invisibility could be reached for frequencies in the microwave-to-terahertz range. In contrast, stealth technology is designed to make objects of military interest as black as possible to radar where, using impedance matching (*14*), electromagnetic waves are absorbed without reflection, i.e., without any echo detectable by radar. Recently, nanofabricated metamaterials with custom-made plasmon resonances have been demonstrated (*13*) that operate in the visible range of the spectrum and may be modified to reach invisibility.

The method used here is general and also applicable to other forms of wave propagation—for example, to sound waves, where the index n describes the ratio of the local phase velocity of the wave to the bulk value, or to quantum-mechanical matter waves, where external potentials act like refractive-index profiles (*1*). For instance, one could use the profiles of n described here to protect an enclosed space from any form of sonic tomography. This study examines the simplest nontrivial case of invisibility, an effectively two-dimensional situation, by applying conformal mapping (*15*) to solve the problem—an elegant technique used in research areas as diverse as electrostatics (*14*), fluid mechanics (*16*), classical mechanics (*17*–*20*), and quantum chaos (*21*, *22*).

Consider an idealized situation: a dielectric medium that is uniform in one direction and light of wave number k that propagates orthogonal to that direction. In practice, the medium will have a finite extension and the propagation direction of light may be slightly tilted without causing an appreciable difference to the ideal case. The medium is characterized by the refractive-index profile $n(x,y)$. To satisfy the validity condition of geometrical optics, $n(x,y)$ must not vary by much over the scale of an optical wavelength $2\pi/k$ (*1*). To describe the spatial coordinates in the propagation plane, complex numbers $z = x + iy$ are used with the partial derivatives $\partial_x = \partial_z + \partial_{z^*}$ and $\partial_y = i\partial_z - i\partial_{z^*}$, where the asterisk symbolizes complex conjugation. In the case of a gradually varying refractive-index profile, both amplitudes ψ of the two polarizations of light obey the Helmholtz equation (*1*)

$$(4\partial_{z^*}\partial_z + n^2k^2)\,\psi = 0 \qquad (1)$$

written here in complex notation with the Laplace operator $\partial_x^2 + \partial_y^2 = 4\partial_{z^*}\partial_z$. Suppose we introduce new coordinates w described by an analytic function $w(z)$ that does not depend on z^*. Such functions define conformal maps (*15*) that preserve the angles between the coordinate lines. Because $\partial_{z^*}\partial_z = |dw/dz|^2\partial_{w^*}\partial_w$, we obtain in w space a Helmholtz equation with the transformed refractive-index profile n' that is related to the original one as

$$n = n'\left|\frac{dw}{dz}\right| \qquad (2)$$

Suppose that the medium is designed such that $n(z)$ is the modulus of an analytic function $g(z)$. The integral of $g(z)$ defines a map $w(z)$ to new coordinates where, according to Eq. 2, the transformed index n' is unity. Consequently, in w coordinates, the wave propagation is indistinguishable from empty space where light rays propagate along straight lines. The medium performs an optical conformal mapping to empty space. If $w(z)$ approaches z for $w \to \infty$, all incident waves appear at infinity as if they have traveled through empty space, regardless

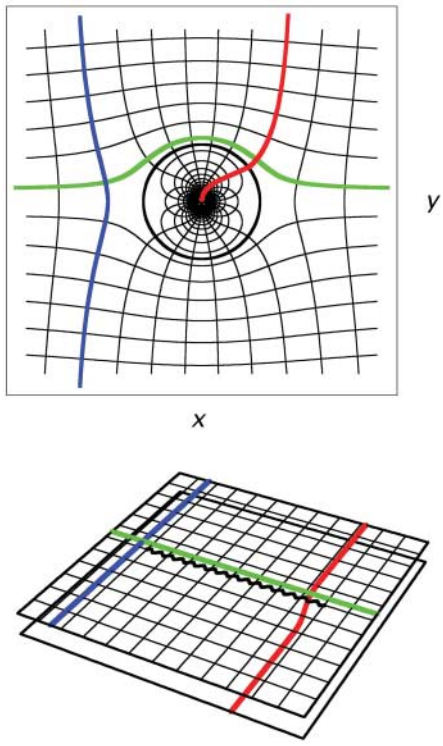

Fig. 1. Optical conformal map. A dielectric medium conformally maps physical space described by the points $z = x + iy$ of the complex plane onto Riemann sheets if the refractive-index profile is $|dw/dz|$ with some analytic function $w(z)$. The figure illustrates the simple map (3) where the exterior of a circle in the picture above is transformed into the upper sheet in the lower picture, and the interior of the circle is mapped onto the lower sheet. The curved coordinate grid of the upper picture is the inverse map $z(w)$ of the w coordinates, approaching a straight rectangular grid at infinity. As a feature of conformal maps, the right angles between the coordinate lines are preserved. The circle line in the figure above corresponds to the branch cut between the sheets below indicated by the curly black line. The figure also illustrates the typical fates of light rays in such media. On the w sheets, rays propagate along straight lines. The rays shown in blue and green avoid the branch cut and hence the interior of the device. The ray shown in red crosses the cut and passes onto the lower sheet where it approaches ∞. However, this ∞ corresponds to a singularity of the refractive index and not to the ∞ of physical space. Rays like this one would be absorbed, unless they are guided back to the exterior sheet.

School of Physics and Astronomy, University of St Andrews, North Haugh, St Andrews KY16 9SS, Scotland. E-mail: ulf@st-andrews.ac.uk

of what has happened in the medium. However, as a consequence of the Riemann Mapping Theorem (*15*), nontrivial w coordinates occupy Riemann sheets with several ∞, one on each sheet. Consider, for example, the simple map

$$w = z + \frac{a^2}{z}, \quad z = {}^1\!/_2\left(w \pm \sqrt{w^2 - 4a^2}\right) \quad (3)$$

illustrated in Fig. 1, that is realized by the refractive-index profile $n = |1 - a^2/z^2|$. The constant a characterizes the spatial extension of the medium. The function (3) maps the exterior of a circle of radius a on the z plane onto one Riemann sheet and the interior onto another. Light rays traveling on the exterior w sheet may have the misfortune of passing the branch cut between the two branch points $\pm 2a$. In continuing their propagation, the rays approach ∞ on the interior w sheet. Seen on the physical z plane, they cross the circle of radius a and approach the singularity of the refractive index at the origin. For general $w(z)$, only one ∞ on the Riemann structure in w space corresponds to the true ∞ of physical z space and the others to singularities of $w(z)$. Instead of traversing space, light rays may cross the branch cut to another Riemann sheet where they approach ∞. Seen in physical space, the rays are irresistibly attracted toward some singularities of the refractive index. Instead of becoming invisible, the medium casts a shadow that is as wide as the apparent size of the branch cut. Nevertheless, the optics on Riemann sheets turns out to serve as a powerful theoretical tool for developing the design of dielectric invisibility devices.

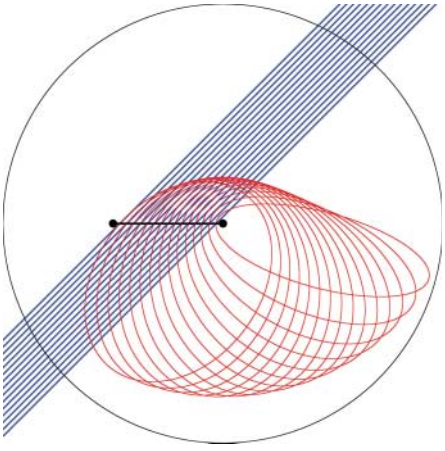

Fig. 2. Light guiding. The device guides light that has entered its interior layer back to the exterior, represented here using two Riemann sheets that correspond to the two layers, seen from above. Light on the exterior sheet is shown in blue and light in the interior, in red. At the branch cut, the thick line between the two points in the figure (the branch points), light passes from the exterior to the interior sheet. Here light is refracted according to Snell's law. On the lower sheet, the refractive-index profile (5) guides the rays to the exterior sheet in elliptic orbits with one branch point as focal point. Finally, the rays are refracted back to their original directions and leave on the exterior sheet as if nothing has happened. The circle in the figure indicates the maximal elongations of the ellipses. This circle limits the region in the interior of the device that light does not enter. The outside of the circle corresponds to the inside of the device. Anything beyond this circle is invisible.

All we need to achieve is to guide light back from the interior to the exterior sheet, i.e., seen in physical space, from the exterior to the interior layer of the device. To find the required refractive-index profile, we interpret the Helmholtz equation in w space as the Schrödinger equation (*1*) of a quantum particle of effective mass k^2 moving in the potential U with energy E such that $U - E = -n'^2/2$ (*1*). We wish to send all rays that have passed through the branch cut onto the interior sheet back to the cut at precisely the same location and in the same direction in which they entered. This implies that we need a potential for which all trajectories are closed. Assuming radial symmetry for $U(w)$ around one branch point w_1, say $+2a$ in our example, only two potentials have this property: the harmonic oscillator and the Kepler potential (*17*). In both cases the trajectories are ellipses (*17*) that are related to each other by a transmutation of force according to the Arnol'd-Kasner theorem (*18–20*). The harmonic oscillator corresponds to a Luneburg lens (*23*) on the Riemann sheet with the transformed refractive-index profile

$$n'^2 = 1 - \frac{|w - w_1|^2}{r_0^2} \quad (4)$$

where r_0 is a constant radius. The Kepler potential with negative energy E corresponds to an Eaton lens (*23*) with the profile

$$n'^2 = \frac{r_0}{|w - w_1|} - 1 \quad (5)$$

Note that the singularity of the Kepler profile in w space is compensated by the zero of $|dw/dz|$ at a branch point in physical space such that the total refractive index (2) is never singular. In both cases (4) and (5), r_0 defines the radius of the circle on the interior w sheet beyond which n'^2 would be negative and hence inaccessible to light propagation. This circle should be large enough to cover the branch cut. The inverse map $z(w)$ turns the outside of the circle into the inside of a region bounded by the image $z(w)$ of the circle line in w space. No light can enter this region. Everything inside is invisible.

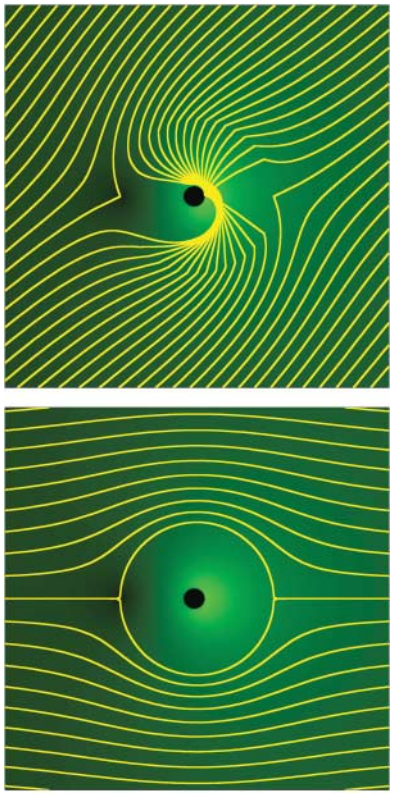

Fig. 3. Ray propagation in the dielectric invisibility device. The light rays are shown in yellow. The brightness of the green background indicates the refractive-index profile taken from the simple map (3) and the Kepler profile (5) with $r_0 = 8a$ in the interior layer of the device. The invisible region is shown in black. The upper panel illustrates how light is refracted at the boundary between the two layers and guided around the invisible region, where it leaves the device as if nothing were there. In the lower panel, light simply flows around the interior layer.

Yet there is one more complication: Light is refracted (*1*) at the boundary between the exterior and the interior layer. Seen in w space, light rays encounter here a transition from the refractive index 1 to n'. Fortunately, refraction is reversible. After the cycles on the interior sheets, light rays are refracted back to their original directions (Fig. 2). The invisibility is not affected, unless the rays are totally reflected. According to Snell's Law (*1*), rays with angles of incidence θ with respect to the branch cut enter the lower sheet with angles θ' such that $n'\sin\theta' = \sin\theta$. If $n' < 1$, this equation may not have real solutions for θ larger than a critical angle Θ. Instead of entering the interior layer of the device, the light is totally reflected (*1*). The angle Θ defines the acceptance angle of the dielectric invisibility device, because beyond Θ, the device appears silvery instead of invisible. The transformed refractive-index profiles (4) and (5) at the boundary between the layers are lowest at the other branch point w_2 that limits the branch cut, $w_2 = -2a$, in our example. In the case of the harmonic-oscillator profile (4), n' lies always below 1, and we obtain the acceptance angle

$$\Theta = \arccos\left(\frac{|w_2 - w_1|}{r_0}\right) \quad (6)$$

For all-round invisibility, the radius r_0 should approach infinity, which implies that the entire

interior sheet is used for guiding the light back to the exterior layer. Fortunately, the Kepler profile (5) does not lead to total reflection if $r_0 \geq 2|w_2 - w_1|$. In this case, the invisible area is largest for

$$r_0 = 2|w_2 - w_1| \quad (7)$$

Figure 3 illustrates the light propagation in a dielectric invisibility device based on the simple map (3) and the Kepler profile (5) with $r_0 = 8a$. Here n ranges from 0 to about 36, but this example is probably not the optimal choice. One can choose from infinitely many conformal maps $w(z)$ that possess the required properties for achieving invisibility: $w(z) \sim z$ for $z \to \infty$ and two branch points w_1 and w_2. The invisible region may be deformed to any simply connected domain by a conformal map that is the numerical solution of a Riemann-Hilbert problem (*16*). We can also relax the tacit assumption that w_1 connects the exterior to only one interior sheet, but to m sheets where light rays return after m cycles. If we construct $w(z)$ as $af(z/a)$ with some analytic function $f(z)$ of the required properties and a constant length scale a, the refractive-index profile $|dw/dz|$ is identical for all scales a. Finding the most practical design is an engineering problem that depends on practical demands. This problem may also inspire further mathematical research on conformal maps in order to find the optimal design and to extend our approach to three dimensions.

Finally, we ask why our scheme does not violate the mathematical theorem (*3*) that perfect invisibility is unattainable. The answer is that waves are not only refracted at the boundary between the exterior and the interior layer, but also are reflected, and that the device causes a time delay. However, the reflection can be substantially reduced by making the transition between the layers gradual over a length scale much larger than the wavelength $2\pi/k$ or by using anti-reflection coatings. In this way, the imperfections of invisibility can be made as small as the accuracy limit of geometrical optics (*1*), i.e., exponentially small. One can never completely hide from waves, but can from rays.

References and Notes

1. M. Born, E. Wolf, *Principles of Optics* (Cambridge Univ. Press, Cambridge, 1999).
2. G. Gbur, *Prog. Opt.* **45**, 273 (2003).
3. A. I. Nachman, *Ann. Math.* **128**, 531 (1988).
4. E. Wolf, T. Habashy, *J. Mod. Opt.* **40**, 785 (1993).
5. M. Kerker, *J. Opt. Soc. Am.* **65**, 376 (1975).
6. A. Alu, N. Engheta, *Phys. Rev. E* **72**, 016623 (2005).
7. D. R. Smith, J. B. Pendry, M. C. K. Wiltshire, *Science* **305**, 788 (2004).
8. R. A. Shelby, D. R. Smith, S. Schultz, *Science* **292**, 77 (2001).
9. J. B. Pendry, *Phys. Rev. Lett.* **85**, 3966 (2000).
10. A. Grbic, G. V. Eleftheriades, *Phys. Rev. Lett.* **92**, 117403 (2004).
11. T. J. Yen *et al.*, *Science* **303**, 1494 (2004).
12. S. Linden *et al.*, *Science* **306**, 1351 (2004).
13. A. N. Grigorenko *et al.*, *Nature* **438**, 335 (2005).
14. J. D. Jackson, *Classical Electrodynamics* (Wiley, New York, 1998).
15. Z. Nehari, *Conformal Mapping* (McGraw-Hill, New York, 1952).
16. M. J. Ablowitz, A. S. Fokas, *Complex Variables* (Cambridge Univ. Press, Cambridge, 1997).
17. L. D. Landau, E. M. Lifshitz, *Mechanics* (Pergamon, Oxford, 1976).
18. V. I. Arnol'd, *Huygens & Barrow, Newton & Hooke* (Birkhäuser Verlag, Basel, 1990).
19. T. Needham, *Am. Math. Mon.* **100**, 119 (1993).
20. T. Needham, *Visual Complex Analysis* (Clarendon, Oxford, 2002).
21. M. Robnik, *J. Phys. A* **16**, 3971 (1983).
22. M. Robnik, M. V. Berry, *J. Phys. A* **19**, 669 (1986).
23. M. Kerker, *The Scattering of Light* (Academic Press, New York, 1969).

24. I am grateful to L. Boussiakou, L. Davila-Romero, M. Dennis, M. Dunn, G. Gbur, C. Gibson, J. Henn, and A. Hindi for the discussions that led to this paper. My work has been supported by the Leverhulme Trust and the Engineering and Physical Sciences Research Council.

21 February 2006; accepted 26 April 2006
Published online 25 May 2006;
10.1126/science.1126493
Include this information when citing this paper.

Controlling Electromagnetic Fields

J. B. Pendry,[1]* D. Schurig,[2] D. R. Smith[2]

Using the freedom of design that metamaterials provide, we show how electromagnetic fields can be redirected at will and propose a design strategy. The conserved fields—electric displacement field D, magnetic induction field B, and Poynting vector B—are all displaced in a consistent manner. A simple illustration is given of the cloaking of a proscribed volume of space to exclude completely all electromagnetic fields. Our work has relevance to exotic lens design and to the cloaking of objects from electromagnetic fields.

To exploit electromagnetism, we use materials to control and direct the fields: a glass lens in a camera to produce an image, a metal cage to screen sensitive equipment, "blackbodies" of various forms to prevent unwanted reflections. With homogeneous materials, optical design is largely a matter of choosing the interface between two materials. For example, the lens of a camera is optimized by altering its shape so as to minimize geometrical aberrations. Electromagnetically inhomogeneous materials offer a different approach to control light; the introduction of specific gradients in the refractive index of a material can be used to form lenses and other optical elements, although the types and ranges of such gradients tend to be limited.

A new class of electromagnetic materials (*1*, *2*) is currently under study: metamaterials, which owe their properties to subwavelength details of structure rather than to their chemical composition, can be designed to have properties difficult or impossible to find in nature. We show how the design flexibility of metamaterials can be used to achieve new electromagnetic devices and how metamaterials enable a new paradigm for the design of electromagnetic structures at all frequencies from optical down to DC.

Progress in the design of metamaterials has been impressive. A negative index of refraction (*3*) is an example of a material property that does not exist in nature but has been enabled by using metamaterial concepts. As a result, negative refraction has been much studied in recent years (*4*), and realizations have been reported at both GHz and optical frequencies (*5*–*8*). Novel magnetic properties have also been reported over a wide spectrum of frequencies. Further information on the design and construction of metamaterials may be found in (*9*–*13*). In fact, it is now conceivable that a material can be constructed whose permittivity and permeability values may be designed to vary independently and arbitrarily throughout a material, taking positive or negative values as desired.

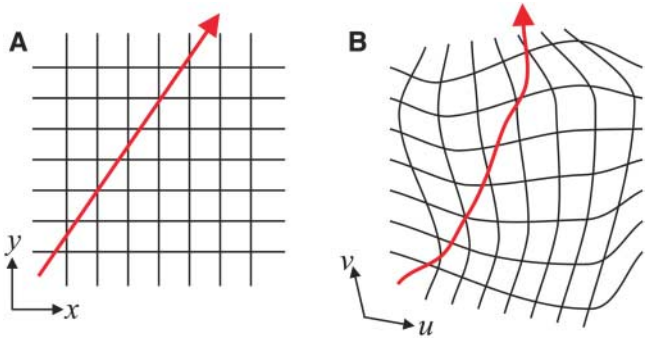

Fig. 1. (**A**) A field line in free space with the background Cartesian coordinate grid shown. (**B**) The distorted field line with the background coordinates distorted in the same fashion. The field in question may be the electric displacement or magnetic induction fields **D** or **B**, or the Poynting vector **S**, which is equivalent to a ray of light.

[1]Department of Physics, Blackett Laboratory, Imperial College London, London SW7 2AZ, UK. [2]Department of Electrical and Computer Engineering, Duke University, Box 90291, Durham, NC 27708, USA.

*To whom correspondence should be addressed. E-mail: j.pendry@imperial.ac.uk